Fabrication of nanozeolite-Y/chitosan composite based on rice husks for efficient adsorption of methylene blue dye: kinetic and thermodynamic studies

Amany G. Braish[1] · Asaad F. Hassan[1] · Shimaa A. El-Essawy[1] · Mohsen M.T. El-Tahawy[1]

Abstract

In this work, three solid adsorbents were synthesized, namely, nanozeolite-Y prepared from rice husks ash by a sol-gel method as a green biosource (ZN), chitosan as a cationic biopolymer (CS), and nanozeolite-Y/chitosan composite (CSZ). An eco-friendly composite that consists of chitosan and nanozeolite-Y was used to combine the advantages of nanoparticles with biopolymers two materials to increase the removal % of methylene blue dye. All the synthetized solid adsorbents were investigated using TGA, nitrogen adsorption, SEM, TEM, FTIR, XRD, and zeta potential. The results showed that CSZ particles had a high specific surface area (432.3 m^2/g), mesoporosity (with an average pore diameter of 2.59 nm), a smaller TEM particle size (between 28.6 and 60.7 nm), a lot of chemical functional groups, and high thermal stability. CSZ exhibited the maximum adsorption capacity (141.04 mg/g) towards methylene blue. The adsorption nature of methylene blue onto CS and CSZ is endothermic, spontaneous, and a physical adsorption process, while it is exothermic, nonspontaneous, physical adsorption process in the case of ZN, as confirmed by thermodynamic results. Pseudo-second order, Elovich, Dubinin-Radushkevich, Freundlich, Langmuir, Temkin, and adsorption models all fit the MB adsorption well, with correlation coefficients reaching about 0.9997. Nitric acid was found to be the best desorbing agent, with a desorption efficiency of about 99%.

Keywords Nanozeolite-Y · Chitosan · Rice husks · Methylene blue · Adsorption

1 Introduction

Wastewater discharge without sufficient treatment causes substantial environmental hazards. Water pollution affects the health of billions of people, inhibits global economic progress, and has an adverse effect on climate change. Due to industrial activity, population growth, and human behavior, environmental contamination has significantly increased (El Nemr, Shoaib et al. [18], Najafi, Abednatanzi et al. [45]). The industry of dyes releases a lot of wastes into the environment, which has the potential to poison both humans and animals (Abdulridha, Jiao et al. [1], Rehan, Rasee et al. [51]). The presence of pigments in the body can have extremely harmful effects on humans who consume large amounts of water. These effects include gastrointestinal distress, vomiting, chest pain, diarrhea, dyspnea, excessive sweating, intense headaches, and cyanosis, in addition to skin irritation and itching (El Nemr, Shoaib et al. [18]). Methylene blue (MB) [3, 7-bis (dimethyl amino) phenothiazine chloride tetra methylthionine chloride] is one of the synthetic dyes used as a coloring agent for papers, wool, silk, and cotton. Due to the unique stability of the aromatic ring in the MB molecular structure, the substance is both carcinogenic and non-biodegradable. The health hazards related to MB include genitourinary, respiratory, cardiovascular, central nervous system disorders, and dermatological impacts (Oladoye, Ajiboye et al. [46]). As a result, before the effluent is dominated in the water system, the dyes must be removed from it to the necessary levels.

✉ Asaad F. Hassan
asmz68@sci.damu.edu.eg

✉ Mohsen M.T. El-Tahawy
mohsen.eltahawy@sci.dmu.edu.eg

[1] Chemistry Department, Faculty of Science, Damanhour University, Damanhour, Egypt

Advanced wastewater treatment techniques frequently involve chemical advanced reduction processes and photocatalysis (Zhou, Yu et al. [64]), physical procedures such as membrane filtration (Zhou, Xiao et al. [65] and ion exchange (Lahiri, Zhang et al. [40]), biological as microbial degradation (Tomar, Kahandawala et al. [61]), physicochemical ozonation (Oladoye, Ajiboye et al. [47]), electrochemical oxidation, advanced oxidation processes (Hama Aziz, Mustafa et al. [23]), and adsorption processes (Zhou, Yu et al. [64]). Adsorption is regarded as one of the most appealing and adaptable treatment approaches due to its simplicity, great efficacy, cheap cost, and low energy usage. Activated carbons (Kumar, Pandey et al. [39]), zeolites, alumina, silica gel (Gupta, Prajapati et al. [21]), natural materials as wood, coal, chitin/chitosan, and clay (Ahmed, Hameed and Hummadi [4]), and nanomaterials have all been considered as dye removal adsorbents. However, some of them have problems such as difficulty in big consumption, regeneration, and limited effective life, necessitating the development of novel adsorbents with high practicability. Because of the unique qualities of nanomaterials, such as a higher number of active sites and a larger surface area, nanomaterials have recently received increased interest in the removal of organic dyes. They can be changed with a variety of chemical groups to improve their chemical affinity for target chemicals. Many nanomaterials, including silicon nanoparticles, carbon nanotubes, nanoclay, nanofibers, polymer-based nanomaterials, and aerogels, have been used in adsorption (Hassan, El-Naggar et al. [27]). The removal of synthetic organic dyes from water and wastewater has been effectively carried out by natural nanomaterials, such as nanozeolites, because of their intrinsic qualities (ion exchange capacity, high chemical stability, meso and microporosity, high surface area, and unique electronic behavior) and size-dependency (Oviedo, Oviedo et al. [49]).

Zeolite nanoparticles (ZN) are crystalline compounds made up of AlO_4 and SiO_4 that have been connected to an ordered system to produce a consistent crystal structure. Two faujasite (FAU) varieties of zeolites that are of particular interest are zeolite-X and zeolite-Y. The ratio of silica to alumina, which is 2:4 for zeolite-X and more than 3 for zeolite-Y, serves as a means of identification (Hassan, Alafid and Hrdina [25]). Specifically, the faujasite (FAU) Y zeolite is considered one of the most widely used zeolites because it has a spherical super cage with a diameter of 1.3 nm and a three-dimensional pore structure with a window aperture of around 0.74 nm (Abdulridha, Jiao et al. [1]). Nanosilica is utilized to adsorb dyes because it is non-toxic, chemically stable, has large specific surface area, and is spherical, all of which provide more adsorption sites for organic molecules (Du, Zhang et al. [15]). Bagasse ash (Oliveira, Cunha and Ruotolo [48]), rice husks ash, coal fly ash (Boycheva,

Marinov et al. [10]), and bamboo leaf (Ahmad, Daou et al. [2]) are all biomass sources of silica for zeolite synthesis. The main components of the by-product from a rice mill are rice straw, rice plant materials, rice husks, etc. Rice husks ash is composed of 4–12% carbon, 85–95% silica (Si), and other residues of metal oxides. Rice husks (RH) have high surface area and a porous, crystalline structure that ranges from 70 to 100 m^2/g, bulk density of 0.25 to 0.30 g/cm^3, and it can hold twice as much water as it weighs. All of these characteristics make the RH a low-cost, high-efficiency filter (Pillai, Dharaskar and Pandian [50]). Making an adsorbent with a high adsorption capacity, performance, selectivity, quick adsorption kinetics, and reusability is a challenge in the adsorption process [52].

Chitosan (CS) is a cationic biopolymer made up of D-glucosamine units and is prepared by the alkaline N-deacetylation of chitin. Chitin is found in the shells of crustaceans, insects, and other organisms. Some of the great chemical and biological properties of CS are that it is biocompatible, has high chemical reactivity, is non-toxic, biodegradable, hydrophilic, has the ability to adsorb, chelate, be chiral, and be antibacterial. The hydroxyl (-OH) and amino ($-NH_2$) groups in the CS chain serve as possible adsorption sites for a variety of water contaminants, including medicines, dyes, and metal ions. The physicochemical characteristics of CS have been described via a variety of techniques, including crosslinking, grafting, and compositing. The crosslinking reaction is the most efficient strategy of these techniques for enhancing the mechanical and chemical stability of CS. For the removal of dyes from aqueous solutions, cross-linked CS adsorbents are frequently used. Zeolite has the negative charge of oxygen connected to aluminum atoms in the framework, which may be connected with chitosan. Zeolite/chitosan composites are getting more focus in the field of pollutants removal from wastewater, such as the adsorption of methyl orange, Fe^{3+}, Ni^{2+}, and Cr^{6+} ions, and humic acid. Chitosan-epichlorohydrin/zeolite composite (CHS-ECH/ZL) is an example of a composite that is used to extract MB dye from aqueous environments. For MB and reactive red 120 (RR120) at 30 °C, the measured adsorption capacities of CHS-ECH/ZL are 156.1 and 284.2 mg/g, respectively [37]. A magnetic sodium alginate-modified zeolite (SA/zeolite/Fe_3O_4) composite with an adsorption capacity of 181.9 mg/g is another example of removing MB from wastewater (Liu, Li and Zhou [42]).

This work aims to discuss the preparation of nanozeolite-Y (ZN) using silica nanoparticles extracted from rice husks (RH) by sol-gel method and its modification with chitosan (CS) for synthesizing nanozeolite composite (CSZ). The synthesized adsorbents were investigated by different physicochemical tools such as XRD, TGA, TEM, SEM, FTIR, zeta potential, and N_2 adsorption/desorption. Batch

adsorption of methylene blue was studied under various adsorption conditions, considering the effects of dosage, pH, temperature, initial concentration, and shaking time of the adsorbate. Both thermodynamics and kinetics parameters were investigated to identify the mechanism and nature of methylene blue adsorption.
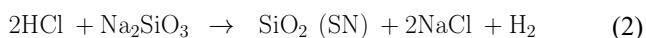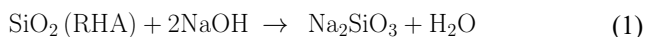
2 Materials and methods

2.1 Materials

Rice husks were gathered from a local rice mill (Damanhour, Egypt). Sodium aluminate was purchased from Sigma-Aldrich Co., Ltd., USA. Sodium hydroxide and hydrochloric acid were obtained from El-Nasr for the chemical and pharmaceutical industry Co., Egypt. Chitosan was purchased from Alfa-Aesar Co., Germany. Methylene blue (MB) and acetic acid were obtained from Piochem Co., Egypt. All chemicals were used without further treatment.

2.2 Solid adsorbents preparation

2.2.1 Preparation of nanosilica from rice husks (SN)

Rice husks (RH) were ignited at 800 °C to a constant weight, and the disappearance of the gray color indicated the production of rice husks ash (RHA). RHA (20 g) was refluxed with 30 mL of 2.0 M HCl for 4.0 h at 120 °C under magnetic stirring. The separated solid residue was washed numerous times with distilled water followed by drying at 110 °C. For five hours, the previously dried solid residue was refluxed in 2.5 M NaOH with constant magnetic stirring. The obtained colorless viscous residue (sodium metasilicate, Eq. 1) was allowed to cool down. In a Teflon beaker, 5.0 M HCl was added drop by drop to the previous viscous solution until the pH reached 2, followed by the dropwise addition of NH_4OH till pH 8.7, and nanosilica particles were formed according to Eq. 2. Then, the nanosilica particles were cleansed using hot distilled water and subsequently dried at a temperature of 120 °C (SN) (Hassan, Alafid and Hrdina [25]):

$$SiO_2 (RHA) + 2NaOH \rightarrow Na_2SiO_3 + H_2O \qquad (1)$$

$$2HCl + Na_2SiO_3 \rightarrow SiO_2 (SN) + 2NaCl + H_2 \qquad (2)$$

2.2.2 Preparation of nanozeolite-Y (ZN)

Zeolite-Y nanoparticles were fabricated based on methods described by Bortolatto et al. and Rahman et al. with slight modifications (Wan Nik, Hasnida and Rahman [63],

Bortolatto, Boca Santa et al. [9], Hassan, Alafid and Hrdina [25]). Sodium silicate (Na_2SiO_3) was prepared from SN nanoparticles by dissolving SN in 2.5 M NaOH under heating and continuous stirring. Two Teflon beakers were prepared: the first one contained 10 mL of 5.09 M sodium hydroxide and 2.09 g of sodium aluminate, while the second one contained 10 mL of 5.09 M sodium hydroxide and 22.72 g of sodium silicate. The two solutions were stirred and allowed to develop for 20 h until they became homogenous. The silicate solution was combined with the aluminate solution and stirred for 6 h until a solidified gel product was formed. The gel was heated, cooled, then rinsed with water till pH 9, centrifuged, and dried overnight at 70 °C. Finally, zeolite-Y nanoparticles were produced and stored in clean, dry bottles.

2.2.3 Preparation of chitosan beads (CS)

Chitosan insoluble beads were produced by dissolving 2.0 g of solid chitosan in 150 mL of 2% aqueous acetic acid for 2 h under continuous stirring. The final solution was dropped with a fine syringe into a 2 M NaOH solution, and the resulting precipitate was filtered and washed several times with distilled water before drying at 70 °C for 24 h (CS) [30].

2.2.4 Preparation of nanozeolite-Y/chitosan composites (CSZ)

Nanozeolite-Y/chitosan composite was produced by dissolving 2 g of chitosan in 150 mL of 2% aqueous acetic acid for 2 h while stirring. A certain weight of the produced nanozeolite-Y was separately suspended in 25 mL of distilled water using a sonication technique and then transferred to a chitosan solution. The previous mixture was stirred constantly for 6 h to ensure homogenous mixing and dropped into a 200 mL, 2 M solution of NaOH. After filtering and washing with distilled water, the solid composite was left to dry overnight at 70 °C (CSZ).

2.3 Characterization of the prepared solid adsorbents

Thermal, textural, and chemical characterization methods are important for evaluating the characteristics of solid adsorbent.

Thermogravimetric analysis (TGA) was performed for RH, SN, ZN, CS, and CSZ to determine the thermal behavior of the samples that were produced using a thermal analyzer apparatus (SDT Q600 V20.9 Build 20) up to 800 °C.

All samples (SN, ZN, CS, and CSZ) were determined for S_{BET} (specific surface area, m²/g), V_T (total pore volume, cm³/g), and $\bar{r}$ (average pore diameter, nm) utilizing nitrogen

adsorption at − 196 °C using a NOVA2000 gas sorption analyzer (Quantachrome Corporation, USA).

X-ray diffraction analysis (XRD) for SN, ZN, CS, and CSZ was performed using a D8 Advance diffractometer for studying the crystal structures and particle size of solid adsorbents. X-ray examinations were performed by using a thin powder sample deposited onto an oriented monocrystalline quartz plate for exposure to a Cu Kα X-ray source (λ = 1.5406 Å). The source of radiation operates at a current of 40 mA and 40 kV with nickel-filtered radiation. The solid samples were evaluated at room temperature over the 2θ range of 10°–50°.

The fabricated solid materials (SN, ZN, CS, and CSZ) were investigated using a Fourier transform infrared spectrometer (FTIR) between 400 and 3800 cm^{-1} range utilizing Mattson 5000 FTIR spectroscopy. Zeta potentials for all adsorbents were determined by Zetasizer Nano S, Malvern Instruments, UK.

Scanning electron microscopy (SEM) was used to determine the morphological structure of (SN, ZN, CS, and CSZ) as solid adsorbents using a JEOL-JSM-7500 F instrument. The samples' surfaces were vacuum evaporated to apply a thin layer of gold (3.5 nm) to reduce the impact of the electron beam on sample charging.

Transmission electron microscope (TEM) was examined for SN, ZN, CS, and CSZ as solid adsorbents through a JEOL-JEM-2100 (Tokyo, Japan). The samples were dried in an oven at 110 °C and dispersed in an anhydrous ethanol solution under ultrasonication for 15 min before being placed on Cu grid and coated with lacey carbon film.

2.4 Batch adsorption of methylene blue (MB)

Batch experiments for the adsorption of MB onto the surfaces of ZN, CS, and CSZ were performed through various application conditions to determine the maximum adsorption capacities, the optimum adsorption conditions, thermodynamic parameters, and kinetic parameters.

Adsorption of MB from aqueous solution at the surface of samples was investigated by mixing 50 mL of MB solution with a known mass of adsorbents (0.1 g) at pH 6.5 for 30 h as a shaking time at 20 °C. The solution was filtered with Whatman filter paper grade 1, where the first five milliliters of filtrate were rejected, and the residual concentration of methylene blue was determined by a UV-vis spectrophotometer (λ_{max} = 662 nm).

The capacity of adsorption q_e (mg/g) at equilibrium was calculated using the following equation:

$$q_e = \frac{(C_0 - C_e) \times V}{W} \tag{3}$$

where C_o and C_e are the starting and equilibrium concentrations of the dye (mg/L), respectively, W is the mass of solid adsorbent (g), and V (L) is the solution volume of MB.

Different adsorption conditions were employed to study the adsorbent dosage (0.2–2.4 g/L), pH (2 − 12), contact time (0.25–25.0 h), initial adsorbate concentration (25–700 mg/L) according to the adsorbent adsorption capacity, and applied adsorption temperature effect (20, 30, 40, and 47 °C). The removal percent (R%) of MB dye was calculated using Eq. 4.

$$Removal\ percent\ (R\%) = \frac{C_0 - C_e}{C_0} \times 100 \tag{4}$$

2.5 Models of adsorption isotherm

To study the availability of MB adsorption on the surface of solid adsorbents, a variety of isotherms have been used in adsorption systems, such as the Langmuir, Freundlich, Temkin, and Dubinin-Radushkevich models.

2.5.1 Langmuir adsorption model

The Langmuir model is applied to the monolayer adsorption of adsorbate onto a finite number of equivalent localized sites of homogenous surface of adsorbent with no interaction between adsorbates and can be represented by Eq. 5.

$$\frac{C_e}{q_e} = \frac{1}{K_L q_m} + \frac{C_e}{q_m} \tag{5}$$

where the maximum adsorption capacity (q_m) and equilibrium adsorption capacity (q_e) are, respectively, expressed in mg/g. The Langmuir adsorption constant is K_L (L/mg).

The dimensionless separation factor (R_L) was calculated to give information on the feasibility of MB adsorption.

$$R_L = \frac{1}{1 + K_L C_0} \tag{6}$$

Herine, R_L value shows the nature of adsorption to be favorable in the case of $0 < R_L < 1$, unfavorable when R_L is greater than 1, linear if $R_L = 1$, and irreversible in the case of $R_L = 0$.

2.5.2 Freundlich adsorption model

This model illustrates the reversible nature of the adsorption technique and describes monolayer and multilayer adsorption on heterogeneous solid surfaces:

$$Ln \, q_e \, = \, Ln \, K_F \, + \, \frac{1}{n} \, Ln \, C_e \tag{7}$$

where K_F and n denote constants associated with the adsorption intensity and capacity, respectively (Shaltout, El-Naggar et al. [55]).

2.5.3 Temkin adsorption model

The Temkin model (Eq. 8) shows the effect of indirect adsorbate–adsorbent interactions; the heat of adsorption decreases linearly rather than logarithmically with surface coverage, and is expressed by:

$$q_e = \beta \, Ln \, K_T + \beta \, Ln \, C_e \tag{8}$$

$$\beta \, = \frac{RT}{b_T} \tag{9}$$

where R is the gas constant (8.314 J/mol. K), T (K) is the Kelvin constant, β is a constant associated with the heat of adsorption, b_T (J/mol) is the Temkin constant, and K_T (L/g) is the Temkin isotherm constant.

2.5.4 Dubinin-radushkevich adsorption model

The model of Dubinin-Radushkevich (Eq. 10) is employed to distinguish between adsorption on heterogeneous and homogeneous surfaces. Compared to the Langmuir type, this isotherm has a more generic nature and can be represented by the following linear equation (Hezma, Shaltout et al. [35]):

$$Ln q_e = Ln q_{DR} - K_{DR} \, \varepsilon^{\,2} \tag{10}$$

$$\varepsilon \, = RTLn \, \left(1 + \frac{1}{C_e} \right) \tag{11}$$

In this case, q_{DR} and K_{DR} are the maximum capacity of adsorption (mg/g) and the D–R constant (mol^2/kJ^2). T, R, and ε denote Kelvin temperature, the gas constant, and the Polanyi potential, respectively. The mean free energy of adsorption (E_{DR}, kJ/mol) is described as:

$$E_{DR} = \frac{1}{\sqrt{2K_{DR}}} \tag{12}$$

2.6 Adsorption kinetic models

Three adsorption kinetic models were investigated for the rate and mechanism of methylene blue adsorption, namely,

pseudo-first order (PFO, Eq. 13), pseudo-second order (PSO, Eq. 15), and Elovich (Eq. 16):

$$Ln \, (q_e - q_t) = Ln \, q_e - k_1 t \tag{13}$$

$$q_t = \frac{(C_0 - C_t \,)}{W} \, \times \, V \tag{14}$$

$$\frac{t}{q_t} \, = \, \frac{1}{K_2 \, q_e^2} \, + \, \frac{1}{q_e} t \tag{15}$$

$$q_t = \frac{1}{\beta} \, Ln \, \alpha \, \, \beta \, + \frac{1}{\beta} \, Ln \, t \tag{16}$$

where C_t (mg/L) is the equilibrium concentration of MB at a certain time (t). k_1 (h^{-1}), k_2 (g/mg.h), and q_t (mg/g) are PFO rate constant, PSO rate constant, and adsorption capacity at time (t), respectively. α (mg/g.h) and β (g/mg) are the initial rate of MB adsorption and activation energy of adsorption, respectively.

2.7 Thermodynamics for methylene blue adsorption

Thermodynamic parameters such as the change in entropy ($\Delta S°$), enthalpy ($\Delta H°$), Gibbs free energy ($\Delta G°$), and equilibrium constant (K_d) were evaluated to study the heat of adsorption, spontaneity, and the ability of MB adsorption on the surface of solid adsorbent nanoparticles. Thermodynamic parameters were determined by using the following equations:

$$K_d = \frac{C_s}{C_e} \tag{17}$$

$$\Delta G^o = \Delta H^o - T \Delta S^o \tag{18}$$

$$Ln \, K_d = \frac{\Delta S^0}{R} \, - \, \frac{\Delta H^0}{RT} \tag{19}$$

Herein, C_e and C_s (mg/L) are the equilibrium concentrations of MB in the solution and on the surface of the adsorbent, respectively. K_d is related to the distribution equilibrium constant of adsorption. The Van't Hoff equation (Eq. 19) enables the calculation of the enthalpy and entropy changes for the adsorption process using the slope and intercept.

2.8 Methylene blue desorption and solid adsorbent reusability

For the desorption study, 0.5 g of CSZ as selected solid adsorbents was mixed with 200 mL of 500 mg/L MB

solution and agitated for 24 h. After the adsorption equilibrium was established, CSZ was filtered, gently washed with an amount of distilled water to eliminate any residual MB and dried at 50 °C. The dried MB pre-loaded CSZ sample was shaken with 50 mL of distilled water, 1 mol/L sodium hydroxide, ethanol (97%), benzene, and nitric acid for 24 h at 45 °C. The desorbed MB concentration was measured in solution after filtration. Desorption efficiency (*D.E*%) was calculated using the given Eq. 20 (Daneshvar, Vazirzadeh et al. [12]):

$$D.E\% = \frac{V\,C_d}{q\,W}\ \times\ 100 \tag{20}$$

where C_d (mg/L) is the concentration of MB solution after desorption from the surface of CSZ. V (L) is the solution volume. q (mg/g) is the maximum adsorbent adsorption capacity. W (g) is the adsorbent mass.

Adsorbent regeneration was performed after six cycles of MB adsorption and desorption runs. Adsorption of MB was tested by CSZ under 2 g/L of adsorbent dose, pH 7, 500 mg/L as MB concentration, 24 h of shaking time, and at 20 °C. After each cycle, the adsorbent was filtered and cleaned several times with 20 mL of nitric acid to desorb the adsorbed MB and dried at 70 °C for successive reuse.

3 Results and discussion

3.1 Characterization of the solid adsorbents

Thermogravimetric analysis (TGA) is a technique that measures the mass of a sample in dependence on temperature. It is particularly effective to examine the thermal stability and purity of solid materials at temperatures ranging from 18 to 800 °C. The prepared materials (RH, SN, ZN, CS, and CSZ) displayed a total loss of mass of 73.4, 6.9, 28.2, 65.5, and 55.8%, respectively, at 800 °C, as shown in Fig. 1a. At 110 °C, all of the samples lost about 3.2% (RH), 1.1% (SN), 6.3% (ZN), 3.8% (CS), and 5.2% (CSZ) wt% of their weight due to the particles' pores evaporating water(Shaltout, El-Naggar et al. [55]). RH has a high level of moisture, indicating the high availability of hydroxyl functional groups on its surface. Severe RH weight loss occurs at about 170 °C and finishes at about 435 °C, and this reduction of about 51.3 wt% is caused by the hemicellulose and cellulose breaking down and releasing volatiles that are extracted from the organic components as condensable vapors (acetic acid, methanol, and wood tar) and incondensable gases (CO, CO_2, CH_4, H_2, and H_2O) released at this point (Saleh, Al-Zaidi and Sabbar [54], F. Hincapié Rojas, Pineda Gómez and Rosales Rivera [20]). The final decomposition of RH occurred between 435

and 800 °C, which is attributed to the formation of residual ash content (Saleh, Al-Zaidi and Sabbar [54]). Additionally, the mass of the nanosilica sample (SN) decreases slowly by only 5.8% up to 800 °C, which could be caused by the desorption of residual moisture, and this may be due to the high porosity of nanosilica, indicating higher thermal stability of SN at high temperatures [24]. The polar nature of the inorganic functional groups of the nanozeolite-Y (ZN) surface is responsible for its higher level of surface moisture adsorption. ZN showed another weight loss from 110 to 240 °C due to the evaporation of water molecules trapped inside the nanozeolite structure (Hassan, Alafid and Hrdina [25]. Another stage of mass loss for ZN occurred between 250 and 800 °C, which was associated with thermal degradation of hydroxyl groups. The thermogravimetric curve of CS showed that 4.1% mass loss occurred in the region of 110–145 °C because of residual water loss. This high temperature (145 °C) can be responsible for the strong hydrogen bonding between water molecules and the active groups (-NH_2 and -OH) of chitosan. From 295 to 350 °C, the glycosidic bonds in chitosan units are degraded, resulting in a weight loss of 7.6%(Habiba, Siddique et al. [22], Kandile, Ahmed et al. [38]). The CSZ composite had a thermal behavior that was in the middle of ZN and CS solids. This was because ZN was mixed into the structure of CS. The residual mass for samples at 800 °C, because of the thermal stability of SN > ZN > CSZ > CS > RH.

The nitrogen adsorption and desorption isotherms are used to examine the structural properties of the synthesized materials, as depicted in Fig. 1b. The solid samples (SN, ZN, and CSZ) showed a type IV adsorption isotherm based on the IUPAC classification, where the adsorption process rises very steeply due to the capillary condensation in mesopores with hysteresis loops of H2 type for ZN and CSZ, but SN displayed a mixture between type H1 and H2 hysteresis loops [24], Hassan, Alafid and Hrdina [25]. CS showed a type II without hysteresis loops appeared, which may be related to its wide pore diameter (4.41 nm). The findings in Table 1 indicate that the specific surface area (S_{BET}) values of ZN > SN > CSZ > CS are 857.2, 804.0, 432.3, and 177.7 m^2/g, respectively, and that observation is evidenced by the total pore volume of ZN > SN > CSZ > CS. The surface area of ZN (857.2 m^2/g) agrees with its lower TEM particle size, which ranged from 5.8 to 13.9 nm. This is based on the fact that as the size of the crystal in the sample decreases, the external surface area increases(Taufiqurrahmi, Mohamed and Bhatia [58]). Also, as appeared in XRD, the peaks are sharp, revealing that ZN has high crystallinity and nanocrystal size, resulting in its high surface area(Shaltout, El-Naggar et al. [55]). The CSZ composite has a larger surface area than CS but a smaller surface area than ZN. This is because some of the inter-particle void volume aggregates
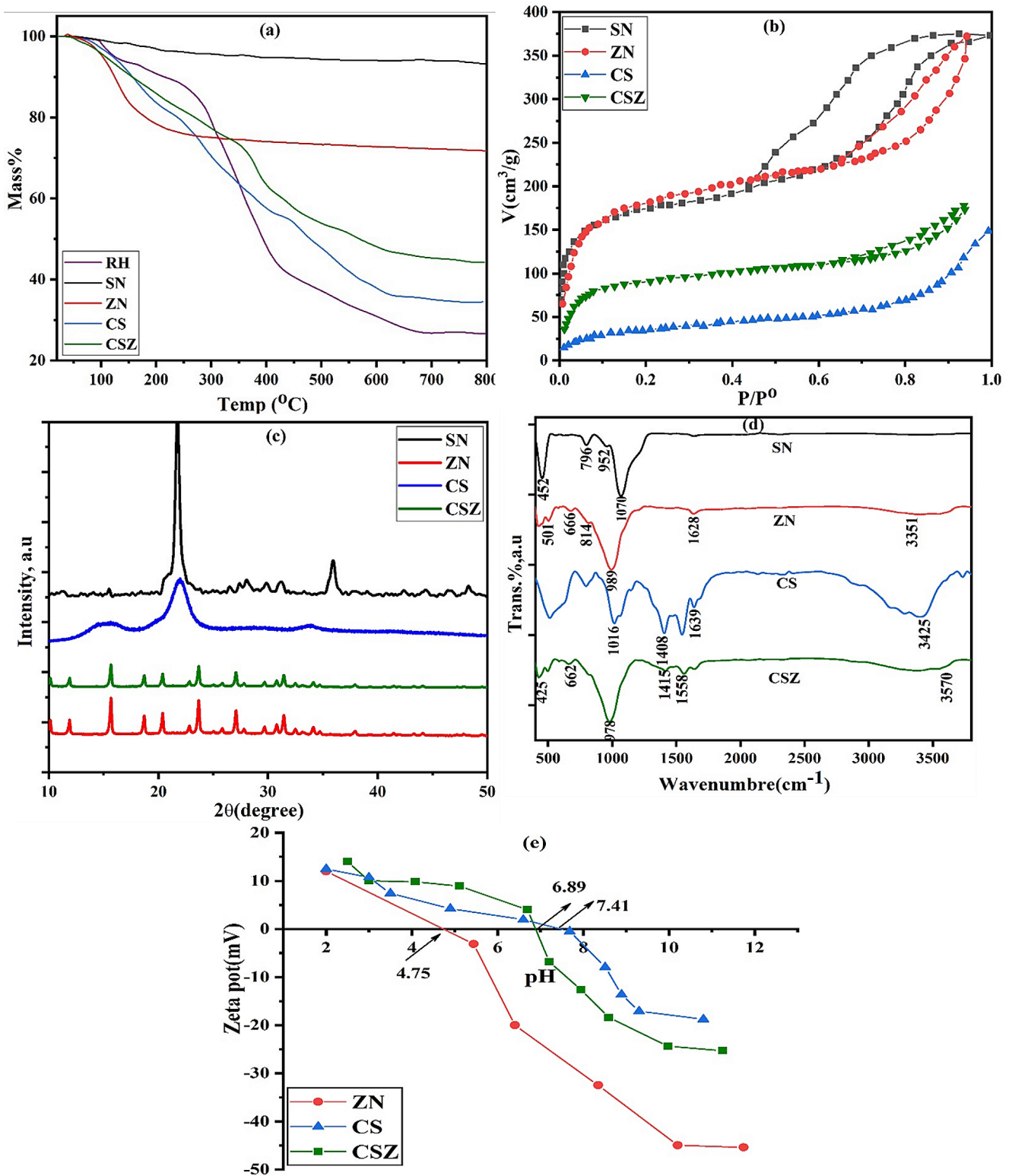
Fig. 1 TGA curves (**a**), nitrogen adsorption/desorption isotherms (**b**), XRD (**c**), FTIR spectra (**d**), and zeta potential (**e**) for RH, SN, ZN, CS, and CSZ

Table 1 Point of zero charge and textural parameters for SN, ZN, CS, and CSZ

Samples	pH_{PZC}	S_{BET} (m^2/g)	V_T (cm^3/g)	$\bar{r}$ (nm)
SN	-----	804.0	0.581	2.89
ZN	4.75	857.2	0.584	2.72
CS	7.41	177.7	0.196	4.41
CSZ	6.89	432.3	0.280	2.59

are filled(Bortolatto, Boca Santa et al. [9]). The average pore diameter ($\bar{r}$, nm) for CS (4.41 nm) > SN (2.89 nm) > ZN (2.72 nm) > CSZ (2.59 nm) indicates the mesoporosity of all the samples (Hassan, Alafid and Hrdina [25].

XRD analysis was used to examine the sample nature and crystal structure of the synthesized adsorbents (SN, ZN, CS, and CSZ), as illustrated in Fig. 1c. The X-ray pattern of the nanosilica portrayed a strong, sharp peak of pure SN centered at $2\theta = 21.7°$, which is compatible with the peak of a characteristic SiO_2 with some less intense peaks at $2\theta = 28.0°$, 29.9°, 31.2°, 36.0°, 42.4°, 44.4°, and 48.3°. The presence of a sharp peak at 21.7° confirms the ordered semi-crystalline structure within the generated silica nanoparticles. The produced silica nanoparticles appeared to sharpen their diffraction peaks due to their smaller particle size and surface defects [24]. Nanozeolite-Y showed characteristic peaks in a crystalline structure located at 2θ values of 10.1°, 11.9°, 15.7°, 18.7°, 20.4°, 23.5°, 27.9°, 31.5°, 34.1°, and 37.9°. According to the XRD analysis, it appears the FAU structure of the ZN sample is attributable to the presence of small crystals (Taufiqurrahmi, Mohamed and Bhatia [59]). Two peaks at $2\theta = 15.3°$ and 21.9° corresponding to (240) and (273), respectively, were visible in the XRD pattern of chitosan (CS), which designates the amorphous structure of the substance (Li, Liu et al. [41]). The CSZ composite is similar to ZN in crystallinity, but it showed a decrease in intensity and shift in peaks compared to ZN, which illustrated an excellent incorporation between ZN and CS.

The prepared samples' chemical bonds and other functional groups can be characterized by FTIR analysis. Figure 1d shows the characteristic symmetry peaks of silica at 796 cm^{-1} and 952 cm^{-1} which can be related to the Si-O-Si stretching vibration, and at 452 cm^{-1}, which belongs to the Si-O-Si bending vibration in the SN sample. The strong and broad peak of asymmetry of Si-O-Si is at 1070 cm^{-1} [33]. Theoretically, the characteristic absorption bands of nanozeolite (ZN) are around 501, 666, 814, 989, 1628, and 3351 cm^{-1}. The peak at 501 cm^{-1} is a characteristic vibration of the internal tetrahedrons of zeolite structures, and the peak at 666 cm^{-1} is due to the presence of double rings in the framework, while the peak at 814 cm^{-1} is sensitive to the Si-Al network composition. The band at 989 cm^{-1} confirms the presence of external asymmetrical stretching of Si–O. The existence of peaks at 1628 and 3351 cm^{-1} is

related to the hydroxyl group of water molecules (Edañol, Usman et al. [16], Hassan, Alafid and Hrdina [25]). The pure CS pattern has a broad crystalline band that corresponds to O–H and N–H stretching. N–H and C-O-H bending and C-O-C stretching are related to the different bands at 1639, 1408, and 1016 cm^{-1}, respectively (Hassan, El-Aziz et al. [32]. The broad band at 3425 cm^{-1}, which is characteristic of chitosan, is attributed to the stretching vibration of the OH group (Habiba, Siddique et al. [22]). Compared to the spectra of ZN and CS, CSZ illustrated the combination of absorbance bands between the CS and ZN groups. The band at 662 cm^{-1} is attributed to the vibration of the external linkage between tetrahedral units, and the peak at 425 cm^{-1} was also observed in the synthesized composite. Some of the characteristic bands of CS were shifted from 1408 to 3425 cm^{-1} to 1415 and 3570 cm^{-1}, respectively, and the peak at 989 cm^{-1} in ZN was shifted to 978 cm^{-1} in composite. The additional absorption band at 1558 cm^{-1} corresponds to O–H, which may be evidence of the mixture of nanozeolite and chitosan.

The chemical surface charge analysis was studied through the zeta potential measurements, which calculated the pH_{PZC} (point of zero charge). The pH_{PZC} values in Table 1 disclose that the pH_{PZC} values of ZN, CS, and CSZ are 4.75, 7.41, and 6.89, respectively, at which the surface has zero charge, as shown in Fig. 1e. Where, at pH values < pH_{PZC} the surface of the adsorbent carries a positive while at pH > pH_{PZC} carry a negative charge.

The surface morphology and shape of the samples (SN, ZN, CS, and CSZ) were identified by SEM and TEM analysis. The scanning electron microscopy (SEM) micrographs of the prepared adsorbents are shown in Fig. 2a-d. The image of nanosilica is uniformly and homogeneously arranged with aggregation [24]. Comparing the analysis of the SEM micrograph with the results from the XRD pattern analysis, it was demonstrated that silica is a semi-crystalline form. ZN showed agglomerated irregular crystals with an octahedral form as well as the formation of pores as a result of nuclei growth (Hassan, Alafid and Hrdina [25]. A picture of chitosan revealed typical dome-shaped orifices, a large surface area, and micro-fibrils in its smooth and non-porous membranous phase (Sinha, Singh and Dutta [57]). The previous characteristics demonstrate the successful encapsulation and good homogeneity of the two solid materials (ZN and CS). The coordination of the chitosan binding sites with the nanozeolite molecules resulted in a noticeable morphological change in the image of the CSZ nanocomposite film. The rough surface of the composite is an important factor in the adsorption because it contributes to high hydrophilicity.

Figure 2e-h show TEM micrographs that provide more precise information on the particle size and surface morphology of the produced samples. The shape of the nanosilica
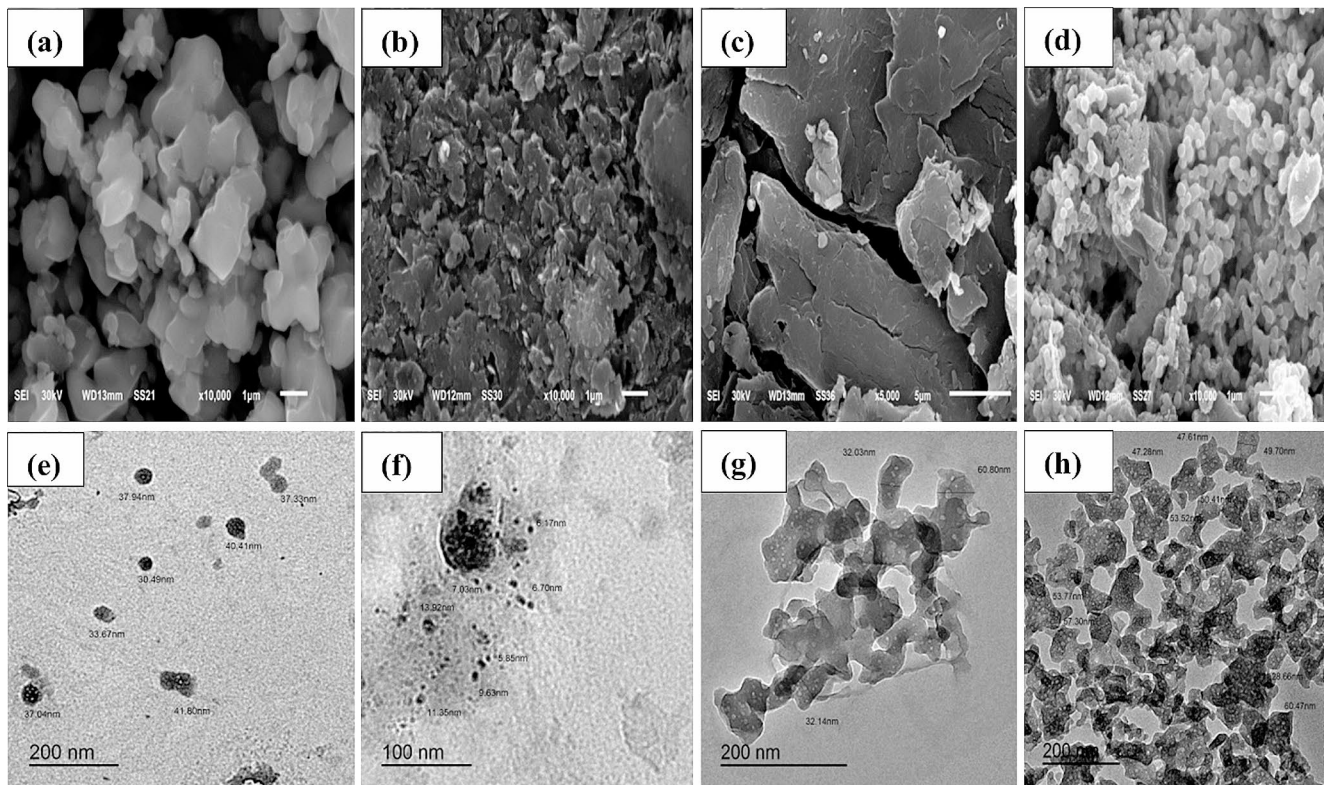
Fig. 2 SEM (**a-d**), and TEM (**e-h**) images for SN, ZN, CS, and CSZ, respectively

is approximately spheroidal, with an average homogenous particle size distribution of around 30.4–41.8 nm and an irregular geometry of the produced particles (Tolba, Barakat et al. [60]). The TEM image of ZN agreed with the features in the SEM image, with a size of 5.8 to 13.9 nm. Chitosan has a fairly uniform and spherical surface shape, with particle sizes ranging from 32.0 to 60.8 nm (Hevira, Ighalo and Sondari [34]). As it appears in the explanation of the composite in SEM analysis, the composite shows a particle size of about 28.6–60.7 nm with white dots, indicating that nanozeolite particles have interfered with the chitosan structure, as evidenced by the smaller size of the ZN and the large surface area of chitosan which indicates the strength of the new composite.

3.2 Adsorption of methylene blue onto all the prepared solid adsorbents

3.2.1 Effect of nanosolid adsorbent dosage

The adsorbent dose is an essential effect that can greatly affect the adsorption of methylene blue on adsorbents. The relation between adsorbent dosages (g/L) and the adsorption capacity (q_e, mg/g) is shown in Fig. 3a, using a dosage range of 0.2 to 2.4 g/L at 20 °C for 24 h of shaking time and 300 mg/L of initial MB concentration. It was observed that

there was a higher increase in adsorption capacity with an increment in the solid dosage from 0.2 for all samples to 1.8 g/L for ZN, 1.0 g/L for CS, and 1.4 g/L for CSZ, where the adsorption capacity increased from 14.3, 38.6, and 60.0 to 64.5, 55.4, and 81.0 mg/g by 4.5, 1.4, and 1.4 times for ZN, CS, and CSZ, respectively, because the adsorbent's surface-active sites increased as the dosage of the adsorbent rose. After this increase, there was no observed increase in MB removal, but a decrease occurred at higher adsorbent doses because the active sites of adsorbents may aggregate during the adsorption reaction, besides the decrease in the MB/active sites ratio (Ezeh, Ogbu et al. [19]). Based on the above results, 2.0 g/L as an adsorbent dose was chosen as the optimum value for the next experiments.

3.2.2 Effect of solution pH

The change in MB adsorption capacity for ZN, CS, and CSZ with pH is displayed in Fig. 3b. The results were studied in a pH range of 2–12 at 20 °C using a 2 g/L adsorbent dose and a 300 mg/L initial MB concentration for 24 h of shaking time. At lower pH levels (pH < pH$_{PZC}$), all solid adsorbents had low q_e values. This was because H$^+$ ions in the solution made it hard for the solid adsorbents to bond with methylene blue. The previous result can be explained on the basis that the hydroxyl group in phase bonded to the
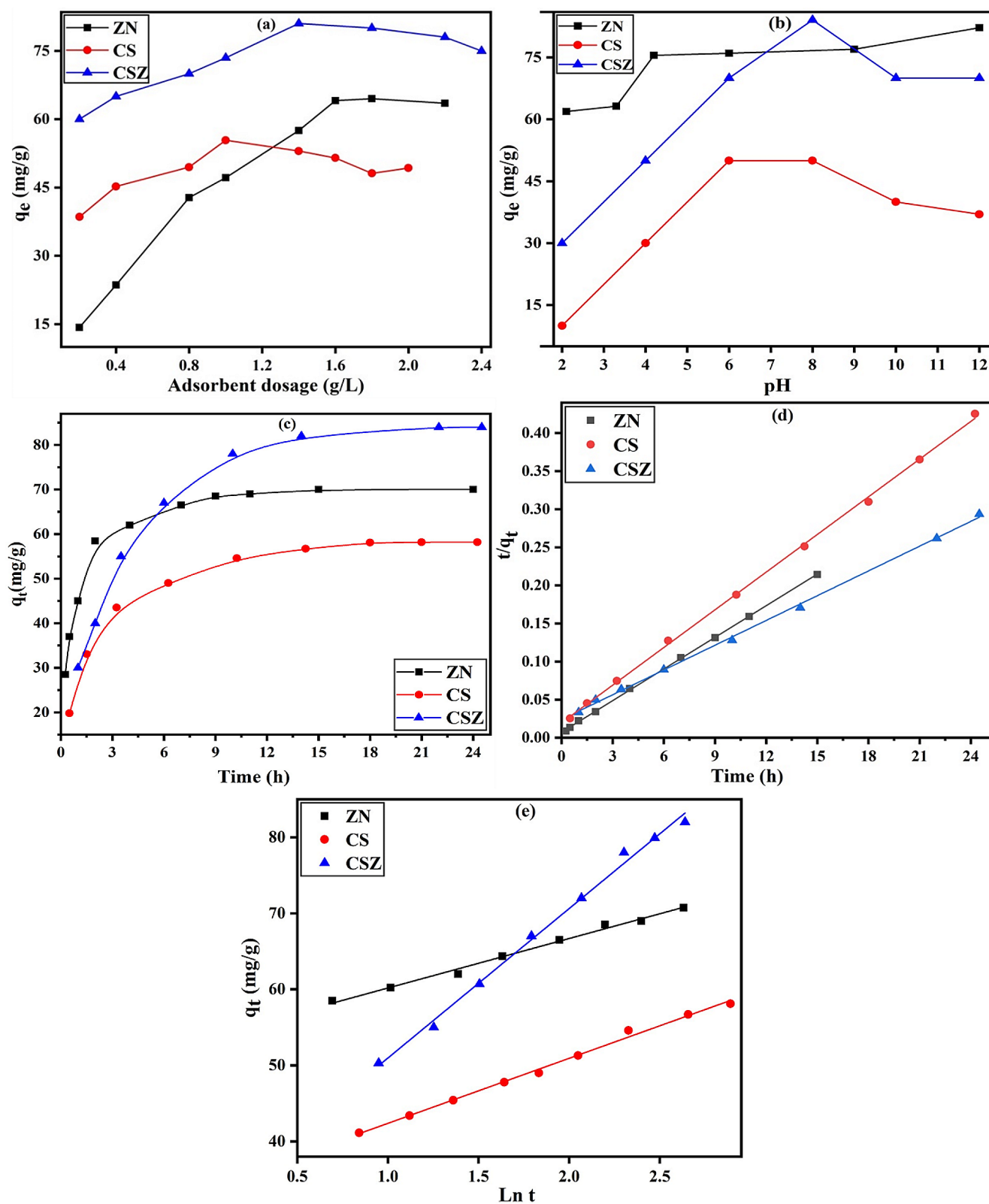
Fig. 3 Effect of dosage (**a**), pH (**b**), contact shaking time (**c**), PSO (**d**), and Elovich (**e**) plots for the adsorption of MB onto ZN, CS, and CSZ at 20 °C

H^+ and became positively charged. Also, the –NH$_2$ in CS and CSZ molecules undergo protonation to generate –$^+$NH$_3$, making it more difficult for the adsorbents to bind to the methylene blue dye cations. The adsorption capacity of MB increased with increasing pH from 2 to 8 for all samples, due to the increase in the electrostatic attraction between adsorbent sites and MB dye (Shaltout, El-Naggar et al. [55]). When the pH was raised from 8 to 12, ZN's ability to absorb dye increased by 6.1%. This was because there were more negatively charged sites on the adsorbent surface, which made the dye stick to it better. In general, as the pH level increased, the net positive charge decreased. This made it easier for the dye to stick to the adsorbent surface, which increased its ability to absorb dye [17]. In the case of CS and CSZ, MB adsorption decreased significantly with an increase in pH from 8 to 12 due to an increase in the number of negative hydroxide ions that compete with adsorbents for the adsorption of methylene blue dye (Anvari, Hosseini et al. [8]). The maximal adsorption capacity for CSZ at pH7 is about 98% at pH 7.9, indicating that the two values are not significantly different. Accordingly, pH = 7 was selected as the optimum pH value for MB adsorption onto all the investigated solid samples.

3.2.3 Effect of time and kinetic study

As shown in Fig. 3c, the plot between adsorption capacity and time determines the shortest time needed for the adsorbent process. The contact shaking time was varied from 0.25 to 25 h at 2 g/L of adsorbent dose, pH 7, 300 mg/L initial dye concentration, and 20 °C. All solid adsorbents displayed a high initial rate of MB adsorption, which increased from 1 to 12 h due to the presence of numerous active sites on their surface. The adsorption rate was slowed down and remained unchanged from 14.0 to 25 h due to the saturation of surface-active sites with MB dye. Based on previous results, 12 h was determined to be the ideal adsorption duration.

Utilizing kinetic models, experimental data has been tested to determine the mechanism of MB adsorption. The parameters of the kinetic models are provided in Table 2. The most often employed models are the pseudo-first order (Eq. 13) and pseudo-second order (Eq. 15) models shown in Fig. S1 and Fig. 3d, respectively, while the Elovich model (Eq. 16) is portrayed in Fig. 3e. According to the result in Table 2 we can conclude that (i) the adsorption of MB onto ZN, CS, and CSZ did not follow the kinetic model of PFO because of the large difference between q_m (Langmuir adsorption capacity) and q_{exp} (adsorption capacity calculated from PFO) values, and the percentage difference between them is 61.7, 38.0 and 16.6% for ZN, CS, and CSZ, respectively. However, the correlation coefficients (R^2, 0.9351–0.9646) are high but less than the correlation coefficient for PSO. (ii) The adsorption of MB onto all three solid adsorbents fitted well to the PSO kinetic model based on its higher R^2 from 0.9985 to 0.9997 and the closer degree between q_m and q_{exp} values by a percentage difference of only 2.8–6.1%.

(iii) The rate constant (k_2) for PSO followed the sequence: ZN (0.0268 g/mg.h) > CS (0.0139 g/mg.h) > CSZ (0.0049 g/mg.h), which may be associated with the strong attraction between ZN and MB. (iv) The correlation coefficients of the Elovich kinetic model were more than 0.9618, revealing the good applicability of this model. Also, the initial rates (α) and the extent of surface coverage (β) sequence of MB adsorption followed the following sequence of ZN > CS > CSZ, indicating an increase in the adsorption equilibrium and surface coverage (Inyinbor, Adekola and Olatunji [36], Alene, Abate and Habte [7], Hassan, Mustafa et al. [31]). Based on the previous study, we can conclude that the

Table 2 PFO, PSO, and Elovich kinetic models and thermodynamic parameters for the MB adsorption onto ZN, CS, and CSZ samples

Models	Parameters		ZN	CS	CSZ
	q_m(mg/g)		78.989	58.997	84.746
PFO	q_{exp}(mg/g)		30.280	36.564	70.640
	k_1(h^{-1})		0.3352	0.3260	0.2723
	R^2		0.9429	0.9351	0.9646
PSO	q_{exp}(mg/g)		74.202	60.643	89.251
	k_2(g/mg.h)		0.0268	0.0139	0.0049
	R^2		0.9997	0.9992	0.9985
Elovich	α (mg/g.h)		24736.5	430.8	93.3
	β (g/mg)		0.1536	0.1161	0.0502
	R^2		0.9843	0.9618	0.9848
Thermodynamic parameters	R^2		0.9972	0.9540	0.9894
	ΔH^o(kJ/mol)		-14.1577	12.4306	8.5946
	ΔS^o(kJ/mol.K)		-0.0511	0.0442	0.0314
	$-\Delta G^o$(kJ/mol)	20 °C	-0.8240	0.5186	0.6194
		30 °C	-1.3353	0.9605	0.9338
		40 °C	-1.8466	1.4024	1.2483
		47 °C	-2.2046	1.7118	1.4684

adsorption of MB onto all solids fits well with the PSO and Elovich models, besides the strong attraction towards the nanozeolite-Y surface.

3.2.4 Effect of the initial concentration of MB and adsorption isotherms

Methylene blue dye adsorption onto the solid adsorbents at 20, 30, 40, and 47 °C was studied using a 2 g/L adsorbent dose and 25–700 mg/L as the initial MB concentration at pH 7 for 12 h as shaking time. The effect of starting concentration of MB on the adsorption capacity of ZN, CS, and CSZ is illustrated in Fig. 4a-c, which shows that the rate of MB adsorption was very high at lower initial concentrations due to a lower number of MB cations to active sites for all adsorbents but eventually became stable at higher initial concentrations, which could be related to active site saturation. The results in Fig. 4a-c indicate that the adsorption capacity increases with an increase in temperature, which indicates the endothermic nature in the case of both CS and CSZ. On the other hand, increasing the temperature reduced the adsorption capacity of ZN, indicating that the adsorption process is exothermic due to the weakening of the attractive forces between the MB dye and the active sites on the adsorbent surface and the fact that an increase in the temperature of the liquid phase will increase the solubility of the adsorbate molecules as well as their diffusion inside the adsorbent pores. Indeed, the adsorption of MB on the ZN surface is favourable at low temperatures (Al-Aoh, Mihaina et al. [6], [5], Salahshour, Shanbedi and Esmaeili [53]).

Various adsorption isotherm models have been used to test the isotherms of Langmuir (Eq. 5), Freundlich (Eq. 7), Temkin (Eq. 8), and Dubinin-Radushkevich (Eq. 10), while the calculated parameters are illustrated in Table 3. Linear Langmuir model and Freundlich model plots for MB adsorption onto ZN, CS, and CSZ at 20, 30, 40, and 47 °C are shown in Fig. 4d-f and Figs. S2a-c, respectively, and the obtained data are listed in Table 3. The results data discussed the higher correlation coefficients from 0.9680 to 0.9972 for the Langmuir model and from 0.9348 to 0.9787 for Freundlich. The adsorption of MB onto all the produced solid samples applied well with the Langmuir and Freundlich adsorption models, indicating the growth of homogeneous monolayer and heterogeneous multilayer adsorption of MB on active sites of solid surfaces. But comparing the Langmuir and Freundlich models we can conclude that the Langmuir ($R^2 > 0.9680$) model is more applicable than the

Freundlich ($R^2 > 0.9348$) model based on the higher correlation coefficient of the Langmuir model (Hassan, El-Naggar et al. [27] Hassan, El-Naggar et al. [28]. The effect of temperature on Langmuir and Freundlich isotherms from 20 to 47 °C explained that MB adsorption is endothermic on the CS and CSZ surface, while MB adsorption onto the ZN surface is exothermic. CSZ adsorption capacity was higher than ZN by 7.3, 107.6, 167.4, and 190.2% at 20, 30, 40, and 47 °C, respectively; this is because the CSZ surface has a higher total pore volume, specific surface area, and rich new surface chemical functional groups, which contribute to attracting MB cations and resulting in an enhanced adsorption process (Hassan, Mustafa et al. [31]). Langmuir binding constant value (K_L, L/mg) was higher in CSZ than those in ZN and CS, revealing the higher binding force between the CSZ surface and MB molecules. The good favorability of MB adsorption onto ZN, CS, and CSZ was indicated by the R_L values from 0.0575 to 0.4064, as shown in Table 3. Additionally, the physical and favorable adsorption process of MB was confirmed by the analyzed $1/n$ values, which ranged between 0.1653 and 0.6370 ($0.1 < 1/n < 1.0$) (Hassan, Alshandoudi and Shaltout [26].

Linear Temkin and Dubinin-Radushkevich (D-R) plots for MB adsorption onto ZN, CS, and CSZ at 20, 30, 40, and 47 °C are shown in Fig. 5a- c and d-f, respectively, and their obtained data are found in Table 3. Concerning the results shown in Table 3, (i) these models well also applied the adsorption of MB onto ZN, CS, and CSZ according to the larger R^2 values ($0.9319 - 0.9993$) for the Temkin model and ($0.9121–0.9981$) for the Dubinin-Radushkevich model. (ii) The range of the Temkin parameter values ($b_T < 8000$ J/mol) from 91.55 to 446.66 J/mol demonstrated the dominance of physical adsorption. (iii) The small difference between (q_m, mg/g) from the Langmuir model and calculated (q_{DR}, mg/g) from Dubinin-Radushkevich, which ranged between 0.02 and 20.66%, supported the good application of the D-R model. According to the assessed E_{DR} values (< 0.0387 kJ/mol), MB is physiosorbed onto ZN, CS, and CSZ, where chemisorption and physisorption processes are accomplished for $8 < E_{DR} < 16$ kJ/mol and $E_{DR} < 8$ kJ/mol, respectively (Hassan, El-Naggar et al. [27]).

3.2.5 Effect of temperature and thermodynamic parameters

Adsorption of MB onto all the prepared solid materials was studied at four temperatures (20, 30, 40, and 47 °C) with an initial concentration of 300 mg/L of dye solution, an amount of adsorbent of 2 g/L, pH 7, and 12 h as shaking time, and the results are shown in Fig. 6a; Table 2. Exothermic or endothermic processes can be determined with their positive or negative enthalpy values ($\Delta H°$)(Doan [14]. The results from
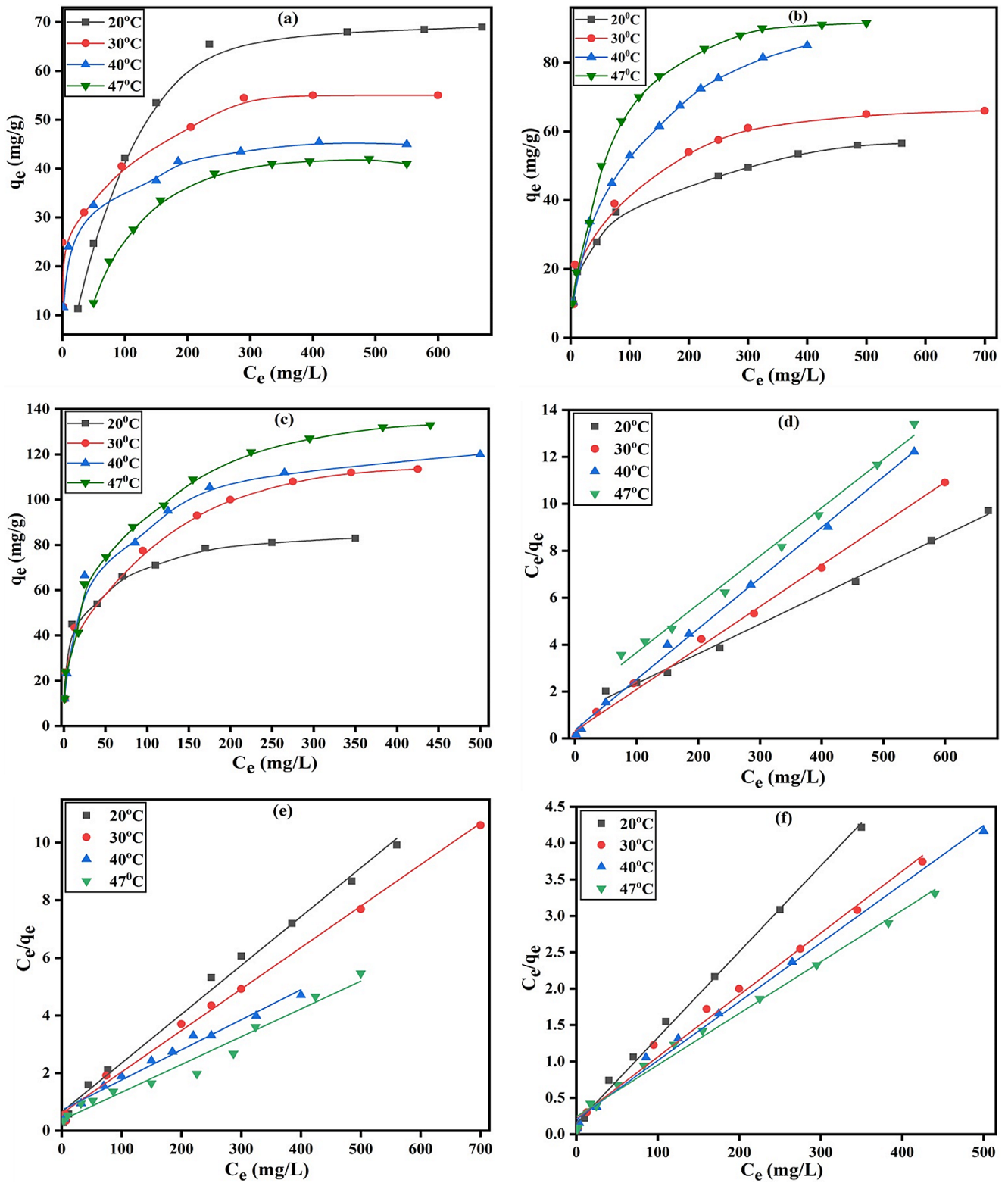
Fig. 4 Adsorption isotherms of MB (**a-c**) and Langmuir plots (**d-f**) for ZN, CS, and CSZ, respectively at 20, 30, 40, and 47 °C

Table 3 Adsorption parameters of Langmuir, Freundlich, Temkin, and Dubinin-Radushkevich for the adsorption of MB onto ZN, CS, and CSZ at 20, 30, 40, and 47 °C

| Parameters	ZN				CS				CSZ			
	20 °C	30 °C	40 °C	47 °C	20 °C	30 °C	40 °C	47 °C	20 °C	30 °C	40 °C	47 °C
Langmuir												
q_m(mg/g)	78.99	56.59	46.34	48.60	58.99	69.44	95.69	103.63	84.76	117.51	123.92	141.04
K_L(L/mg)	0.0117	0.0544	0.0591	0.0128	0.0261	0.0241	0.0146	0.0262	0.0807	0.0403	0.0393	0.0292
R_L	0.0957	0.0693	0.0575	0.1121	0.2771	0.2930	0.4064	0.2761	0.1102	0.1988	0.2028	0.2549
R^2	0.9957	0.9953	0.9972	0.9903	0.9924	0.9962	0.9777	0.9680	0.9957	0.9904	0.9938	0.9906
Freundlich												
1/n	0.6370	0.2614	0.1653	0.4510	0.2808	0.3130	0.3959	0.3505	0.1949	0.2975	0.2305	0.2890
K_F($L^{1/n} \cdot mg^{1-1/n}$/g)	2.123	12.252	16.961	3.182	10.051	10.226	8.522	12.966	28.111	20.229	30.974	24.603
R^2	0.9670	0.9569	0.9565	0.9348	0.9665	0.9693	0.9787	0.9580	0.9685	0.9668	0.9560	0.9446
Temkin												
K_T(L/g)	0.0497	0.8832	5.6756	0.1239	0.7652	0.4880	0.2952	0.3308	3.9793	0.5443	1.1521	0.3679
b_T(J/mol)	91.55	272.22	446.66	242.45	266.08	214.84	153.32	142.45	209.35	119.69	135.97	100.09
R^2	0.9993	0.9461	0.9810	0.9319	0.9809	0.9699	0.9615	0.9709	0.9624	0.9845	0.9527	0.9853
Dubinin-Radushkevich												
q_{DR}(mg/g)	69.94	54.85	46.93	43.02	58.98	67.80	75.92	85.92	83.42	118.86	119.90	134.35
E_{DR}(kJ/mol)	0.0239	0.0334	0.0260	0.0245	0.0143	0.0182	0.0298	0.0382	0.0387	0.0220	0.0301	0.0273
R^2	0.9757	0.9121	0.9520	0.9981	0.9759	0.9844	0.9360	0.9567	0.9968	0.9972	0.9724	0.9881

Table 2 show that the higher correlation coefficient values of the Van't Hoff plot (Eq. 19) for ZN (0.9972), CS (0.9540), and CSZ (0.9894) indicate the good fit of this model as presented in Fig. 6a. The ΔH^o values are − 14.1577, 12.4306, and 8.5946 kJ/mol for ZN, CS, and CSZ, respectively, confirming the exothermic nature of ZN and the endothermic nature of CS and CSZ for MB adsorption onto the prepared samples. The $\Delta S°$ values are 0.0442 kJ/mol.K for CS and 0.0314 kJ/mol.K for CSZ. This means that there was more randomness at the interface between adsorbent and solution during the adsorption process. On the other hand, the ZN value went down by -0.0511 kJ/mol.K, which showed the opposite situation (Al-Aoh, Mihaina et al. [6]). The positive values of ΔG^o for ZN range from 0.8240 to 2.2046 kJ/mol, proving the nonspontaneous nature of MB adsorption onto the ZN surface, and ΔG^o for CS and CSZ range from − 0.5186 to -1.7118 kJ/mol, confirming the spontaneous nature of MB adsorption (Hassan, El-Naggar et al. [27]). Nonspontaneous adsorption of MB on ZN implies that the adsorption process requires extra power to increase the adsorption efficiency.

3.3 Desorption and reusability studies

Desorption studies have provided a qualitative analysis of the reversibility of the adsorption process. Figure 6b demonstrates the use of several eluents for MB desorption from the CSZ adsorbent. The desorption efficiency was calculated using Eq. 20, showing the following trend: nitric acid > sodium hydroxide > ethanol > benzene > distilled water, with percentages desorption of 99, 29, 13, 8, and 6%, respectively. Viscosity, eluent polarity, solubility of MB in eluent, and the number of cations (especially protons) produced from desorbing eluent determine the desorption efficiency values. Nitric acid achieved high desorption of MB, leading to a significant electrostatic repulsion between the highly protonated CSZ surface and the MB cations. Distilled water and benzene showed the lowest desorption percentages, which are due to the small number of positively charged protons produced (Daneshvar, Vazirzadeh et al. [12], Ahmad and Ejaz [3]. The reuse study was performed in six adsorption/desorption cycles and removal efficiency was determined in each cycle. The data also explained that the MB adsorption efficiency of the CSZ composite slightly decreased by 9.5% after six cycles used for MB dye removal, as shown in Fig. S3, and that may be attributed to the CSZ particles' coagulation, resulting in a reduction in surface area and the loss of some chemical functional groups. The regeneration results show that the composite adsorbent maintains its high adsorption efficiency for MB even after numerous recycles [17].
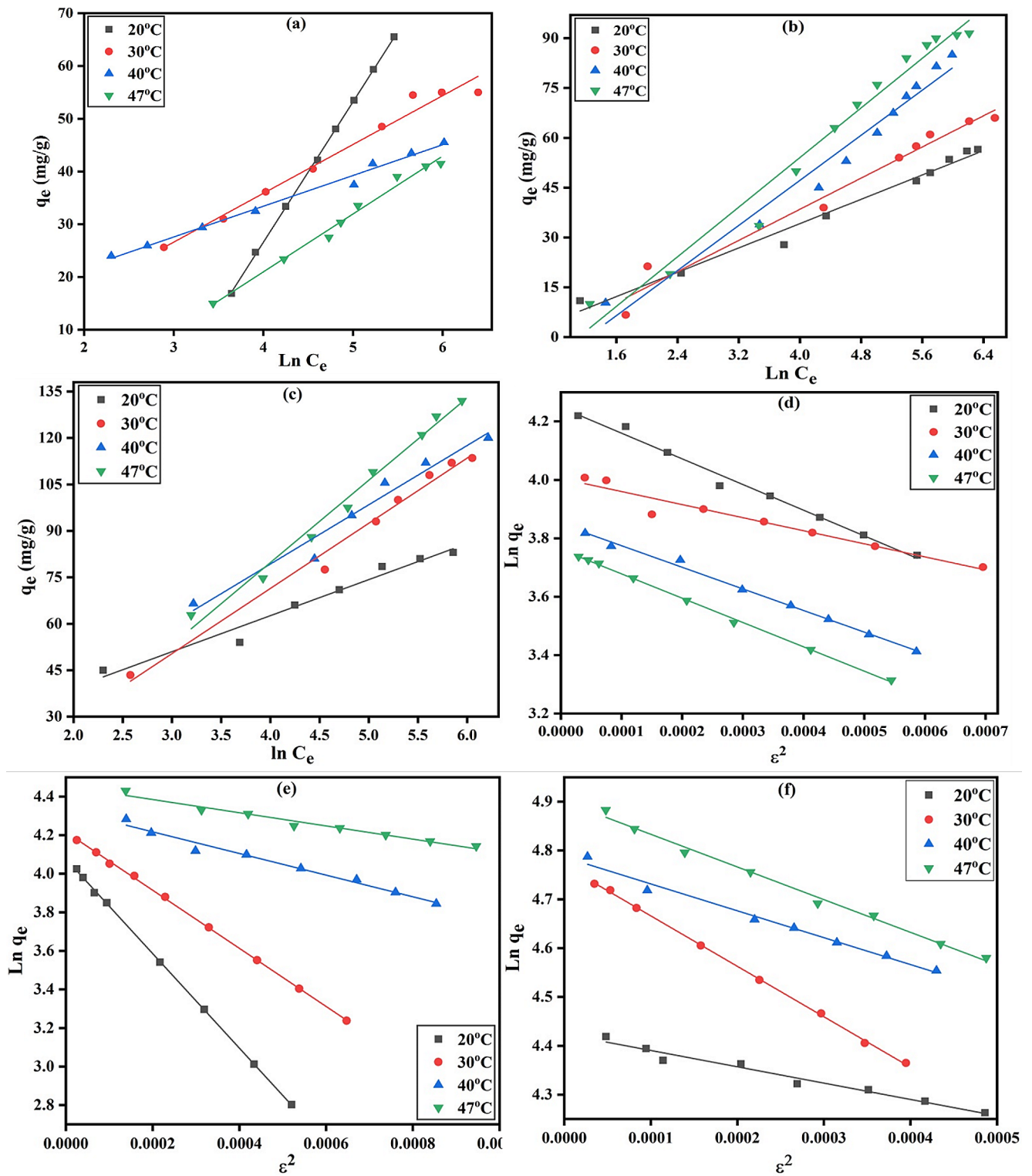
Fig. 5 Temkin (**a-c**) and linear Dubinin–Radushkevich plots (**d-f**) for the adsorption of MB onto ZN, CS, and CSZ, respectively at 20, 30, 40, and 47 °C
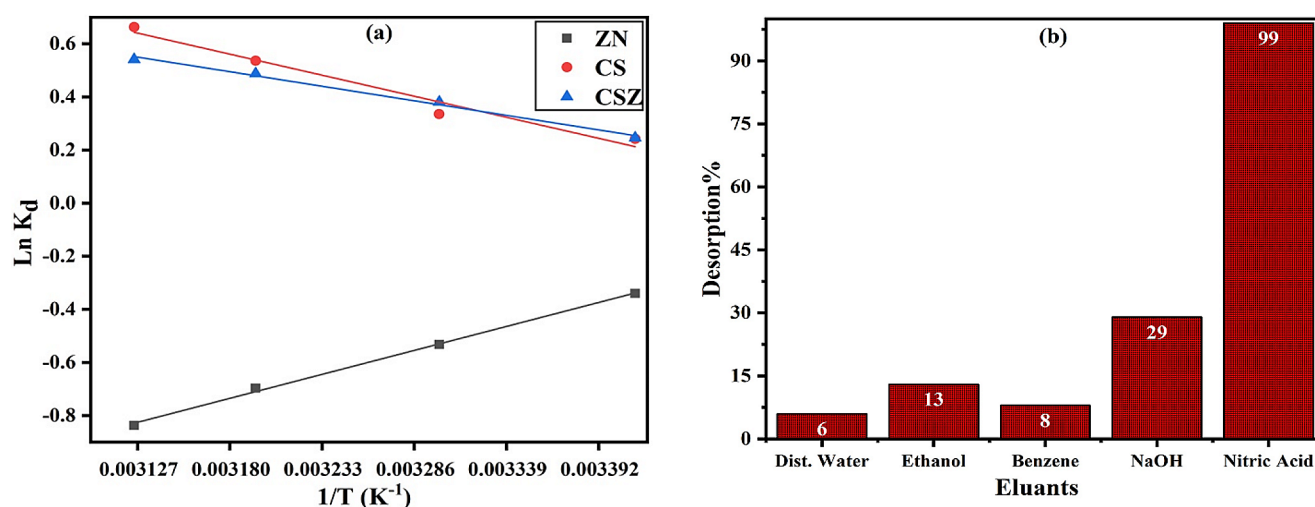
Fig. 6 Van't Hoff plot for all the studied solid adsorbents (**a**) and desorption of MB from CSZ using different solvents (**b**)

Table 4 Maximum adsorption capacity of CSZ in comparison to other composites

Adsorbents	q_m (mg/g)	references
CZC	24.5	[60]
Fe$_3$O$_4$/ZA	40.4	[61]
CCM	45.1	[62]
Chitosan-magadiite beads	45.3	[63]
Zeolite–rGO	53.3	[64]
Zeolite/AC@MnO$_2$	67.6	[65]
CS–ZX aerogels	108.0	[66]
CSZ	141.0	[This study]

3.4 Comparison of CSZ with other adsorbents

In this study, CSZ was compared with other solid materials for MB adsorption, as shown in Table 4 (Zhu, Wang et al. [66], Cho, Jeon et al. [11], Dehghani, Dehghan et al. [13], Mokhtar, Abdelkrim et al. [44] Marotta, Luzzi et al. [43], Tran, Duong et al. [62], Shojaei and Esmaeili [56]. We found that CSZ had the greatest adsorption capacity compared to the other materials, showing that CSZ is an excellent solid adsorbent for MB removal from aqueous solutions.

4 Conclusion

In summary, rice husks were used to synthesize silica nanoparticles which were used in the preparation of nanozeolite-Y (ZN) and nanozeolite-Y/chitosan composite (CSZ) was resulted from the combination of the ZN nanoparticles and the prepared chitosan (CS). Characterization investigations by different techniques: TGA, nitrogen adsorption, SEM, TEM, FTIR, XRD, and Zeta potential showed CSZ composite with a total mass loss of 55.8% at 800 °C, higher surface area (432.3 m^2/g), pH$_{PZC}$ (6.89), porous structure, richness with chemical functional groups, and crystalline structure. Sample dose, shaking time, pH, starting MB concentration, temperature, and other essential experimental parameters were established, and experimental results have been recorded. Adsorption of MB onto all the prepared solid materials was investigated, where CSZ exhibited higher adsorption capacities towards MB dye and increased from 84.76 to 141.04 mg/g by raising the temperature from 20 to 47 °C, utilizing 2 g/L of adsorbent dosage, 12 h of shaking time, and pH 7. Kinetic studies prove the good applications of PSO and Elovich models. The Langmuir, Freundlich, Temkin, and Dubinin-Radushkevich adsorption isotherms were good at describing how MB stuck to all the solid adsorbents that were made. Thermodynamic studies showed that MB spontaneously and endothermically attached to CS and CSZ, but ZN did not adhere spontaneously and exothermically. Nitric acid played an essential role in the desorption of MB from the solid surface by about 99%. The higher reusability of CSZ was tested after six cycles of MB adsorption and desorption and exhibited a decrease in its adsorption capacity of only 9.5%. Lastly, methylene blue and other organic colors may be effectively removed from wastewater using the CSZ composite made of nanozeolite Y and chitosan.

Author contributions S.A.E. conducted the primary research, including synthesis, characterization, and experiments. A.G.B. assisted with the experimental work and characterization techniques and wrote the initial draft. A.F.H. and M.M.T.E. co-supervised the project, provided guidance on experimental design, and contributed to the interpretation of data. They also co-wrote and revised the manuscript.

Data availability No datasets were generated or analysed during the current study.

Declarations

References

1. Abdulridha, S., Jiao, Y., Xu, S., Zhang, R., Ren, Z., Garforth, A.A., Fan, X.: A comparative study on Mesoporous Y zeolites prepared by hard-templating and post-synthetic treatment methods. Appl. Catal. A. **612**, 117986 (2021)

2. Ahmad, N.H., Daou, T.J., Maireles-Torres, P., Zaarour, M., Mintova, S., Ling, T.-C., Ng, E.-P.: Morphological effects on catalytic performance of LTL zeolites in acylation of 2-methylfuran enhanced by non-microwave instant heating. Mater. Chem. Phys. **244**, 122688 (2020)

3. Ahmad, R., Ejaz, M.O.: Synthesis of new alginate-silver nanoparticles/mica (Alg-AgNPs/MC) bionanocomposite for enhanced adsorption of dyes from aqueous solution. Chem. Eng. Res. Des. **197**, 355–371 (2023)

4. Ahmed, M.J., Hameed, B.H., Hummadi, E.H.: Review on recent progress in chitosan/chitin-carbonaceous material composites for the adsorption of water pollutants. Carbohydr. Polym. **247**, 116690 (2020)

5. Ait Hmeid, H., Baghour, A.M.M., Moumen, A., Skalli, A., Daoudi, L., Aalaoul, M., Azizi, G., Anjjar, A.: Adsorption of a basic dye, Methylene Blue. Aqueous Solut. Bentonite. **9**, 416–433 (2021)

6. Al-Aoh, H.A., Mihaina, I.A.M., Alsharif, M.A., Darwish, A.A.A., Rashad, M., Mustafa, S.K., Aljohani, M.M.H., Al-Duais, M.A., Al-Shehri, H.S.: Removal of methylene blue from synthetic wastewater by the selected metallic oxides nanoparticles adsorbent: Equilibrium, kinetic and thermodynamic studies. Chem. Eng. Commun. **207**(12), 1719–1735 (2019)

7. Alene, A.N., Abate, G.Y., Habte, A.T.: Bioadsorption of Basic Blue Dye from Aqueous Solution onto Raw and Modified Waste Ash as Economical Alternative Bioadsorbent. J. Chem. **2020**, 1–11 (2020)

8. Anvari, S., Hosseini, M., Jahanshahi, M., Banisheykholeslami, F.: Design of chitosan/boehmite biocomposite for the removal of anionic and nonionic dyes from aqueous solutions: Adsorption isotherms, kinetics, and thermodynamics studies. Int. J. Biol. Macromol. **259**(Pt 2), 129219 (2024)

9. Bortolatto, L.B., Boca Santa, R.A.A., Moreira, J.C., Machado, D.B., Martins, M.A.P.M., Fiori, M.A., Kuhnen, N.C., Riella, H.G.: Synthesis and characterization of Y zeolites from alternative silicon and aluminium sources. Microporous Mesoporous Mater. **248**, 214–221 (2017)

10. Boycheva, S., Marinov, I., Miteva, S., Zgureva, D.: Conversion of coal fly ash into nanozeolite Na-X by applying ultrasound assisted hydrothermal and fusion-hydrothermal alkaline activation. Sustainable Chem. Pharm. **15**, 100217 (2020)

11. Cho, D.-W., Jeon, B.-H., Chon, C.-M., Schwartz, F.W., Jeong, Y., Song, H.: Magnetic chitosan composite for adsorption of cationic and anionic dyes in aqueous solution. J. Ind. Eng. Chem. **28**, 60–66 (2015)

12. Daneshvar, E., Vazirzadeh, A., Niazi, A., Kousha, M., Naushad, M., Bhatnagar, A.: Desorption of Methylene blue dye from brown macroalga: Effects of operating parameters, isotherm study and kinetic modeling. J. Clean. Prod. **152**, 443–453 (2017)

13. Dehghani, M.H., Dehghan, A., Alidadi, H., Dolatabadi, M., Mehrabpour, M., Converti, A.: Removal of methylene blue dye from aqueous solutions by a new chitosan/zeolite composite from shrimp waste: Kinetic and equilibrium study. Korean J. Chem. Eng. **34**(6), 1699–1707 (2017)

14. Doan, L.: Modifying Superparamagnetic Iron Oxide nanoparticles as Methylene Blue adsorbents. Rev. ChemEngineering. **7**(5), 77 (2023)

15. Du, P., Zhang, J., Cai, Z., Ge, F.: High adsorption of cationic dyes from aqueous solution using worm-like porous nanosilica: Isotherm, kinetics and thermodynamics. Mater. Today Commun. **35**, 105697 (2023)

16. Edañol, Y.D.G., Usman, K.A.S., Buenviaje, S.J.C., Mantua, M.E., Payawan, L.J.M.: Utilizing silica from Rice Hull for the Hydrothermal synthesis of Zeolite. Y Kimika. **29**(1), 17–21 (2018)

17. El- Maghraby, A., El deeb, H.: Removal of a basic dye from aqueous solution by adsorption using rice hulls. Global NEST J. **13**, 90 (2011)

18. El Nemr, A., Shoaib, A.G.M., El Sikaily, A., Mohamed, A.E.-D.A., Hassan, A.F.: Evaluation of Cationic Methylene Blue Dye Removal by high Surface Area Mesoporous activated Carbon Derived from Ulva lactuca. Environ. Processes. **8**(1), 311–332 (2021)

19. Ezeh, K.A., Ogbu, I.C., Akpomie, K.G., Ojukwu, N.C., Ibe, J.C.: Utilizing the Sorption Capacity of Local Nigerian Sawdust for Attenuation of Heavy Metals from Solution. Isotherm, Kinetic, and Thermodynamic Investigations (2017)

20. Hincapié Rojas, F., Pineda Gómez, D.P., Rosales Rivera, A.: Production and characterization of silica nanoparticles from rice husk. Adv. Mater. Lett. **10**(1), 67–73 (2019)

21. Gupta, S., Prajapati, A., Kumar, A., Acharya, S.: Synthesis of silica aerogel and its application for removal of crystal violet dye by adsorption. Watershed Ecol. Environ. **5**, 241–254 (2023)

22. Habiba, U., Siddique, T.A., Joo, T.C., Salleh, A., Ang, B.C., Afifi, A.M.: Synthesis of chitosan/polyvinyl alcohol/zeolite composite for removal of methyl orange, Congo Red and chromium(VI) by flocculation/adsorption. Carbohydr. Polym. **157**, 1568–1576 (2017)

23. Hama Aziz, K.H., Mustafa, F.S., Omer, K.M., Shafiq, I.: Recent advances in water falling film reactor designs for the removal of organic pollutants by advanced oxidation processes: A review. Water Resour. Ind. **30**, 100227 (2023)

24 Hassan, A.F., Abdelghny, A.M., Elhadidy, H., Youssef, A.M.: Synthesis and characterization of high surface area nanosilica from rice husk ash by surfactant-free sol–gel method. J. Solgel Sci. Technol. **69**(3), 465–472 (2013)

25 Hassan, A.F., Alafid, F., Hrdina, R.: Preparation of melamine formaldehyde/nanozeolite Y composite based on nanosilica extracted from rice husks by sol–gel method: Adsorption of lead (II) ion. J. Solgel Sci. Technol. **95**(1), 211–222 (2020)

26 Hassan, A.F., Alshandoudi, L.M., Shaltout, W.A.: Utilizing modified cellulose nanoparticles derived from a plant loofah sponge to improve the removal of diazinon insecticide from an aqueous medium. RSC Adv. **13**(11), 7280–7292 (2023)

27 Hassan, A.F., El-Naggar, G.A., Braish, A.G., Abd El-Latif, M.M., Shaltout, W.A., Elsayed, M.S.: Fabrication of titania/calcium alginate nanocomposite matrix for efficient adsorption and photocatalytic degradation of malachite green. Int. J. Biol. Macromol. **249**, 126075 (2023)

28 Hassan, A.F., El-Naggar, G.A., Braish, A.G., El-Latif, M.M.A., Shaltout, W.A., Elsayed, M.S.: Utilization of synthesized copper Ferrite/Calcium Alginate Nanocomposite for Adsorption and Photocatalytic Degradation of Malachite Green. J. Inorg. Organomet. Polym Mater. **34**(1), 190–206 (2023)

29 Hassan, A.F., El-Naggar, G.A., Esmail, G., Shaltout, W.A.: Efficient adsorption of methylene blue on novel triple-nanocomposites of potassium Kappa-carrageenan, calcium alginate and nanohydroxyapatite obtained from sea scallop shells. Appl. Surf. Sci. Adv. **13**, 100388 (2023)

30 Hassan, A.F., Hrdina, R.: Chitosan/nanohydroxyapatite composite based scallop shells as an efficient adsorbent for mercuric ions: Static and dynamic adsorption studies. Int. J. Biol. Macromol. **109**, 507–516 (2018)

31 Hassan, A.F., Mustafa, A.A., Esmail, G., Awad, A.M.: Adsorption and Photo-Fenton Degradation of Methylene Blue Using Nanomagnetite/Potassium Carrageenan Bio-composite beads. Arab. J. Sci. Eng. **48**(1), 353–373 (2022)

32 Hassan, S.S.M., El-Aziz, M.E.A., Fayez, A.E., Kamel, A.H., Youssef, A.M.: Synthesis and characterization of bio-nanocomposite based on chitosan and CaCO(3) nanoparticles for heavy metals removal. Int. J. Biol. Macromol. **255**, 128007 (2024)

33 Helmiyati, H., Suci, R.P.: Nanocomposite of cellulose-ZnO/SiO2 as catalyst biodiesel methyl ester from virgin coconut oil. Proceedings of the 4th International Symposium on Current Progress in Mathematics and Sciences (Iscpms2018), AIP Publishing. (2019)

34 Hevira, L., Ighalo, J.O., Sondari, D.: Chitosan-based polysaccharides for effective synthetic dye adsorption. J. Mol. Liq. **393**, 123604 (2024)

35 Hezma, A.M., Shaltout, W.A., Kabary, H.A., El-Bahy, G.S., Abdelrazzak, A.B.: Fabrication, characterization and Adsorption Investigation of Nano Zinc oxide–sodium alginate beads for effective removal of chromium (VI) from aqueous solution. J. Inorg. Organomet. Polym Mater. **33**(5), 1400–1408 (2023)

36 Inyinbor, A.A., Adekola, F.A., Olatunji, G.A.: Kinetics, isotherms and thermodynamic modeling of liquid phase adsorption of rhodamine B dye onto Raphia hookerie fruit epicarp. Water Resour. Ind. **15**, 14–27 (2016)

37 Jawad, A.H., Abdulhameed, A.S., Reghioua, A., Yaseen, Z.M.: Zwitterion composite chitosan-epichlorohydrin/zeolite for adsorption of methylene blue and reactive red 120 dyes. Int. J. Biol. Macromol. **163**, 756–765 (2020)

38 Kandile, N.G., Ahmed, M.E., Mohamed, M.I., Mohamed, H.M.: Therapeutic applications of sustainable new chitosan derivatives and its nanocomposites: Fabrication and characterization. Int. J. Biol. Macromol. **254**(Pt 2), 127855 (2024)

39 Kumar, N., Pandey, A., Rosy, Sharma, Y.C.: A review on sustainable mesoporous activated carbon as adsorbent for efficient removal of hazardous dyes from industrial wastewater. J. Water Process. Eng. **54**, 104054 (2023)

40 Lahiri, S.K., Zhang, C., Sillanpää, M., Liu, L.: Nanoporous NiO@SiO2 photo-catalyst prepared by ion-exchange method for fast elimination of reactive dyes from wastewater. Mater. Today Chem. **23**, 100677 (2022)

41 Li, S., Liu, X., Zhang, X., Fan, L., Wang, F., Zhou, J., Zhang, H.: Preparation and characterization of zein-tannic acid nanoparticles/chitosan composite films and application in the preservation of sugar oranges. Food Chem. **437**(Pt 1), 137673 (2024)

42 Liu, F., Li, W., Zhou, Y.: Preparation and characterization of magnetic sodium alginate-modified zeolite for the efficient removal of methylene blue. Colloids Surf., a. **629**, 127403 (2021)

43 Marotta, A., Luzzi, E., Salzano de Luna, M., Aprea, P., Ambrogi, V., Filippone, G.: Chitosan/Zeolite Composite Aerogels for a fast and effective removal of both Anionic and Cationic dyes from Water. Polym. (Basel). **13**(11), 1691 (2021)

44 Mokhtar, A., Abdelkrim, S., Djelad, A., Sardi, A., Boukoussa, B., Sassi, M., Bengueddach, A.: Adsorption behavior of cationic and anionic dyes on magadiite-chitosan composite beads. Carbohydr. Polym. **229**, 115399 (2020)

45 Najafi, M., Abednatanzi, S., Gohari Derakhshandeh, P., Mollarasouli, F., Bahrani, S., Behbahani, E.S., Van Der Voort, P., Ghaedi, M.: Metal-organic and covalent organic frameworks for the remediation of aqueous dye solutions: Adsorptive, catalytic and extractive processes. Coord. Chem. Rev. **454**, 214332 (2022)

46 Oladoye, P.O., Ajiboye, T.O., Omotola, E.O., Oyewola, O.J.: Methylene blue dye: Toxicity and potential elimination technology from wastewater. Results Eng. **16**, 100678 (2022)

47 Oladoye, P.O., Ajiboye, T.O., Wanyonyi, W.C., Omotola, E.O., Oladipo, M.E.: Ozonation, electrochemical, and biological methods for the remediation of malachite green dye wastewaters: A mini review. Sustainable Chem. Environ. **3**, 100033 (2023)

48 Oliveira, J.A., Cunha, F.A., Ruotolo, L.A.M.: Synthesis of zeolite from sugarcane bagasse fly ash and its application as a low-cost adsorbent to remove heavy metals. J. Clean. Prod. **229**, 956–963 (2019)

49 Oviedo, L.R., Oviedo, V.R., Dalla Nora, L.D., da Silva, W.L.: Adsorption of organic dyes onto nanozeolites: A machine learning study. Sep. Purif. Technol. **315**, 123712 (2023)

50 Pillai, P., Dharaskar, S., Pandian, S.: Rice husk derived silica nano doped on calcium peroxide for fluoride: Performance, characterization, kinetic, isotherm, and groundwater treatment. Environ. Technol. Innov. **19**, 100901 (2020)

51 Rehan, A.I., Rasee, A.I., Awual, M.E., Waliullah, R.M., Hossain, M.S., Kubra, K.T., Salman, M.S., Hasan, M.M., Hasan, M.N., Sheikh, M.C., Marwani, H.M., Khaleque, M.A., Islam, A., Awual, M.R.: Improving toxic dye removal and remediation using novel nanocomposite fibrous adsorbent. Colloids Surf., a. **673**, 131859 (2023)

52 Roshanfekr Rad, L., Anbia, M.: Zeolite-based composites for the adsorption of toxic matters from water: A review. J. Environ. Chem. Eng. **9**(5), 106088 (2021)

53 Salahshour, R., Shanbedi, M., Esmaeili, H.: Methylene Blue Dye removal from aqueous media using activated Carbon prepared by Lotus leaves: Kinetic, equilibrium and thermodynamic study. Acta Chim. Slov. **68**(2), 363–373 (2021)

54 Saleh, N.J., Al-Zaidi, B.Y.S., Sabbar, Z.M.: A comparative study of Y zeolite catalysts derived from natural and commercial silica: Synthesis, characterization, and Catalytic Performance. Arab. J. Sci. Eng. **43**(11), 5819–5836 (2017)

55 Shaltout, W.A., El-Naggar, G.A., Esmail, G., Hassan, A.F.: Synthesis and characterization of ferric@nanocellulose/nanohydroxyapatite bio-composite based on sea scallop shells and cotton stalks: Adsorption of Safranin-O dye. Biomass Convers. Biorefinery. **14**(4), 4759–4776 (2022)

56 Shojaei, M., Esmaeili, H.: Ultrasonic-assisted synthesis of zeolite/activated carbon@MnO(2) composite as a novel adsorbent for treatment of wastewater containing methylene blue and brilliant blue. Environ. Monit. Assess. **194**(4), 279 (2022)

57 Sinha, N., Singh, B., Dutta, P.: Preparation and characterization of Chitosan-Lauric Acid Derivative: Antibacterial Activity and Drug Delivery Study. J. Polym. Mater. **33**, 479–489 (2016)

58 Taufiqurrahmi, N., Mohamed, A.R., Bhatia, S.: Nanocrystalline Zeolite Y: Synthesis and characterization. IOP Conf. Series: Mater. Sci. Eng. **17**, 012030 (2011)

59 Taufiqurrahmi, N., Mohamed, A.R., Bhatia, S.: Nanocrystalline Zeolite Y: Synthesis and characterization. IOP Conf. Series: Mater. Sci. Eng. **17**(1), 012030 (2011)

60 Tolba, G.M.K., Barakat, N.A.M., Bastaweesy, A.M., Ashour, E.A., Abdelmoez, W., El-Newehy, M.H., Al-Deyab, S.S., Kim, H.Y.: Effective and highly recyclable nanosilica produced from the rice husk for effective removal of organic dyes. J. Ind. Eng. Chem. **29**, 134–145 (2015)

61 Tomar, T., Kahandawala, N., Kaur, J., Thounaojam, L., Choudhary, I., Bera, S.: Bioremediation of synthetic dyes from wastewater by using microbial nanocomposites: An emerging field for water pollution management. Biocatal. Agric. Biotechnol. **51**, 102767 (2023)

62 Tran, N.B.T., Duong, N.B., Le, N.L., Mitu, L.: Synthesis and characterization of magnetic Fe3O4/Zeolite NaA nanocomposite for the Adsorption removal of Methylene Blue Potential in Wastewater Treatment. J. Chem. **2021**, 1–14 (2021)

63 Wan Nik, W.B., Hasnida, N., Rahman, M.M.: Preparation of Zeolite Y using local raw Material Rice Husk as a silica source. J. Sci. Res. **1**(2), 285–291 (2009)

64 Zhou, K., Yu, H., Li, Q., liang, D., Luo, J., Yu, Y., Zhang, C., Sun, Y., Wu, C., Cheng, Z.: Application of phosphomolybdate/tungsten disulfide composites in the adsorption and photocatalytic degradation of dyeing wastewater. Sep. Purif. Technol. **330**, 125431 (2024)

65 Zhou, L., Xiao, G., He, Y., Wu, J., Shi, H., Zhong, F., Yin, X., Li, Z., Chen, J.: Multifunctional filtration membrane with anti-viscous-oils-fouling capacity and selective dyes adsorption ability for complex wastewater remediation. J. Hazard. Mater. **413**, 125379 (2021)

66 Zhu, J., Wang, Y., Liu, J., Zhang, Y.: Facile One-Pot synthesis of Novel Spherical Zeolite–reduced Graphene Oxide composites for Cationic Dye Adsorption. Ind. Eng. Chem. Res. **53**(35), 13711–13717 (2014)